J Mater Sci (2008) 43:2123–2130
DOI 10.1007/s10853-007-2033-8

Hydrothermal syntheses, structures and magnetic properties of coordination frameworks of divalent transition metals

Hitoshi Kumagai · Hideo Sobukawa · Mohamedally Kurmoo

Received: 26 October 2006 / Accepted: 20 July 2007 / Published online: 22 December 2007

Abstract The hydrothermal syntheses, single-crystal X-ray structures and magnetic properties of $[Co(C_4O_4)(H_2O)_2]$ (**1**), $[Co_3(OH)_2(C_4O_4)_2] \cdot 3H_2O$ (**2**) and $[Fe(OH)_2(C_4O_4)]$ (**3**) are described. Pale yellow cubes of **1** and brown red crystals of **2** were obtained from the reaction of $Co(OH)_2$ and squaric acid at 200 °C. Brown needle of **3** were obtained similarly from $Fe(SO_4) \cdot 7H_2O$, squaric acid and NaOH. **1** consists of a cubic sodalite arrangement with empty cavities where the Co atoms are connected by μ_4-squarate and two *trans*-water molecules each, while **2** and **3** contain metal-hydroxide double-chains of edge-sharing octahedral, brucite-type for **2** and goethite for **3**, connected by μ_6-squarate. **2** contains water molecules in the channels which can be removed and re-inserted repeatedly without loss of crystallinity. All three compounds possess 3D frameworks made up of coordination and hydrogen bonds. **1** behaves as a paramagnet while **2** and **3** are antiferromagnets and **2** transforms to a ferromagnet reversibly upon dehydration and rehydration. The structures of two one-dimensional polymers employing 2,5-pyridinedicarboxylate, $[Co_2(H_2O)_6(2,5\text{-pydc})_2] \cdot 2H_2O$ (**4**) and Cu (2,5-pydc)$_2$ (**5**), are also reported.

Introduction

Organic-inorganic hybrid materials employing coordination chemistry are of great current interest due to their intriguing structural diversity and potential for dual-function combining superconductivity, non-linear optical property and magnetism [1–6]. They also belong to an important class of materials potential for catalysis, host-guest chemistry and gas sorption [7–11]. Hydrothermal synthesis of these organic-inorganic hybrid materials has proved to be very successful and is now widely used. However, it remains a black art for some reactions. For carboxylate materials much advances have been made in controlling the crystalline phases by choice of solvents, pH, order of adding the reactants and concentrations, temperature and pressures. By tuning these parameters, we have been able to prepare a range of magnetic materials containing various polycarboxylate and transition metals. In particular, we have focused our attentions on several aspects viz. (a) the number of carboxylate groups attached to a benzene backbone ranging from mono- to hexa-carboxylate, [12–19] (b) distances between two carboxylate groups, [20] (c) geometry of the carboxylate for introducing chirality and optical activity, [21–24] and (d) combination of nitrogen and oxygen donor atoms by the use of different pyridine-carboxylates [24b]. Concerning the magnetic properties, we have achieved Curie temperatures of up to 60 K and coercivity of 20 kOe for several ferrimagnets and some unusual metamagnets with coercivity in excess of 50 kOe at 2 K [12, 16, 25–27]. In many cases, the hydrothermal reactions of polycarboxylic acid with M(II) ions were found to result in different phases, [28] where some were found to exhibit permanent porosity and magnetism. In this challenge, the achievement of porosity commonly requires the use of relatively long molecular connecting units, whereas long-range magnetic ordering requires relatively short exchange pathways between nearest neighboring (NN) metal sites, such as M(II)–O–M(II) [22, 28, 29].

H. Kumagai (✉) · H. Sobukawa
Toyota Central R and D Labs. Inc., 41-1 Yokomichi, Nagakute, Aichi-gun, Aichi 480-1131, Japan
e-mail: e1254@mosk.tytlabs.co.jp

M. Kurmoo
Laboratoire de Chimie de Coordination Organique, UMR7140, CNRS Université Louis Pasteur, Institut Le Bel, 4 rue Blaise Pascal, Strasbourg Cedex 67000, France

The oxocarbon anions ($C_mO_n^{-z}$) belong to an interesting class of aromatic ligands having various bridging modes [30–32]. Their complexes with transition metals are well-known for their interesting magnetic and optoelectronic properties. To expand our chemistry, squaric acid is employed in the reaction with Co(II) and Fe(II) under hydrothermal condition. Structural characterizations of several squarate-M(II) coordination networks have been reported. They are $M(C_4O_4)(H_2O)_4$, $M(HC_4O_4)_2(H_2O)_4$ and $M(C_4O_4)(H_2O)_2$ [33–35]. Additional types have been found for $Mn_2(OH)_2(C_4O_4)$, $[Co_3(OH)_2(C_4O_4)_2] \cdot 3H_2O$, $[V(OH)(C_4O_4)(H_2O)]_2$, and $[V(OH)(C_4O_4)]_2$ containing μ_3-bridging hydroxide [36–39]. As mentioned above, the key structural feature with respect to the magnetic properties is the single-atom bridges M(II)–O–M(II). Therefore, for coordination polymers consisting of M(II)-squarate and bridging hydroxide, structures can be expected where permanent porosity and magnetism can co-exist. $[Co_3(OH)_2(C_4O_4)_2] \cdot 3H_2O$ was first to be synthesized and we have demonstrated the reversible ferromagnetic-antiferromagnetic transformation upon dehydration-rehydration of the porous coordination framework [29, 38]. During the synthesis of $[Co_3(OH)_2(C_4O_4)_2] \cdot 3H_2O$, we also obtained $[Co(C_4O_4)(H_2O)_2]$ (**1**). Here, we report the hydrothermal syntheses, structural characterizations and magnetic properties of $[Co(C_4O_4)(H_2O)_2]$ (**1**), $[Co_3(OH)_2(C_4O_4)_2] \cdot 3H_2O$ (**2**) and $[Fe_2(OH)_2(C_4O_4)]$ (**3**). In addition, we also present the synthesis and crystal structures of two one-dimensional coordination polymers employing 2,5-pyridinedicarboxylate bridges, $[Co_2(H_2O)_6(2,5\text{-pydc})_2] \cdot 2H_2O$ (**4**) and $Cu(2,5\text{-pydc})_2$ (**5**).

Experimental

All chemicals were purchased from Tokyo Kasei and Aldrich and were used without further purification. The syntheses were carried out in home-built Teflon-lined cylindrical stainless steel autoclaves with maximum capacity of 40 mL or 120 mL. X-Ray powder diffraction data at room temperature were collected using a flat-plate geometry on a Siemens D-500 equipped with Co-Kα (λ = 1.789 Å) radiation. The temperature and field dependence magnetizations were measured on a Quantum Design MPMS-XL SQUID magnetometer operating in the temperature range 2–300 K and at fields up to 50 kOe. Ac-susceptibilities were measured in field of 1 Oe oscillating at 20 Hz using the same instrument.

Preparation of $[Co(C_4O_4)(H_2O)_2]$ (1) and $[Co_3(OH)_2(C_4O_4)_2] \cdot 3H_2O$ (2)

Freshly prepared $Co(OH)_2$ (0.26 g) and $H_2C_4O_4$ (0.11 g) were suspended in H_2O (ca. 50 mL). The mixture was then placed in a Teflon lined autoclave, sealed and heated to 200 °C for 3 days followed by cooling to 25 °C in a water bath. The yellow crystals of **1** and brown-red crystals of **2** were filtered, washed with water and dried in air. The crystals were separated under a microscope for further characterizations.

Preparation of $[Fe_2(OH)_2(C_4O_4)]$ (3)

$Fe(SO_4) \cdot 7H_2O$ (0.27 g) and $H_2C_4O_4$ (0.11 g) and NaOH (0.10 g) were placed in the Teflon liner of an autoclave and previously boiled and degassed water (30 mL) was added. The mixture was then sealed and heated to 200 °C for 3 days followed by cooling to 25 °C in a water bath. A brown powder and light brown crystals of **3** were filtered, washed with water and dried in air. The crystals were separated from the powder under a microscope for characterizations. Some particles of iron-oxide were separated from the bulk of the crystals by a SmCo magnet.

Preparation of $[Co_2(H_2O)_6(2,5\text{-pydc})_2] \cdot 2H_2O$ (4) and $Cu(2,5\text{-pydc})_2$ (5)

2,5-pyridinedicarboxylic acid (0.57 g) was neutralized with NaOH (0.27 g) in 5 mL of water. Solution of $M(NO_3)_2 \cdot 6H_2O$ (1.0 g) in 10 mL of water was added to the solution. Orange crystals of **4** and blue crystals of **5** were obtained after one week.

X-ray crystallography and structure solution

Selected single crystals were glued on the tip of glass fibers for data collection on a Kappa-CCD Nonius diffractometer equipped with a graphite monochromated Mo-Kα (0.7107 Å) radiation. The data were corrected for Lorentz and polarization effects. The structure was solved by direct methods and expanded using Fourier techniques [40]. The non-hydrogen atoms were refined anisotropically. The final cycle of full-matrix least-squares refinement was based on the number of observed reflections and n variable parameters. They converged (large parameter shift was σ times its e.s.d.) with agreement factors of $R = \sum||F_o| - |F_c||/\sum|F_o|$, $R_w = [\sum w(|F_o| - |F_c|)^2/\sum w\,|F_o|^2]^{1/2}$. No extinction corrections have been applied. The crystal and refinement parameters are summarized in Table 1.

Results and discussion

Crystal structure of **1**

The structure of **1** is shown in Fig. 1. It consists of a cubic arrangement of *trans*-$Co(H_2O)_2$ and squarate dianion. The cobalt atoms have octahedral coordination with four

Table 1 Crystallographic data of the compounds

Compound	**1**	**2**[29]	**3**	**4**	**5**
Empirical formula	$C_4H_4O_6Co$	$C_8H_8O_{13}Co_3$	C_2HO_3Fe	$C_8H_{12}CoNO_8$	$C_8H_3CuNO_4$
Formula weight	207.01	488.94	128.88	309.12	240.66
Crystal system	Cubic	Monoclinic	Monoclinic	Triclinic	Triclinic
Space group	*P* n-3n	C 2/m	$P\ 2_1/c$	$P-1$	$P-1$
a (Å)	16.2442(9)	9.2966(10)	3.3418(2)	7.056(1)	6.9130
b (Å)		12.8636(13)	10.026(1)	8.926(1)	7.3511
c (Å)		5.4998(6)	8.4822(8)	9.658(1)	10.1419
α (°)				90.929(4)	78.7900
β (°)		90.533(2)	99.590(5)	100.750(6)	73.0200
γ (°)				108.077(6)	41.5600
V (Å^3)	4286.4(7)	657.68(12)	280.21(8)	566.3158	
Z	24	2	4	2	
D_c (g cm^{-3})	1.92	2.469	3.05	1.813	
μ (cm^{-1})	2.382	3.816	5.155	1.551	
No. reflns.	306	810	528	2424	
No. params.	51	64	55	166	
R1	0.033 [$I > 3.00\sigma(I)$]	0.027 [$I > 2\sigma(I)$]	0.025 [$I > 3.00\sigma(I)$]	0.0372 [$I > 2.00\sigma(I)$]	
Residual (e/Å^3)	0.555/−0.404	0.781/−0.623	0.585/−0.860	1.03/−0.70	

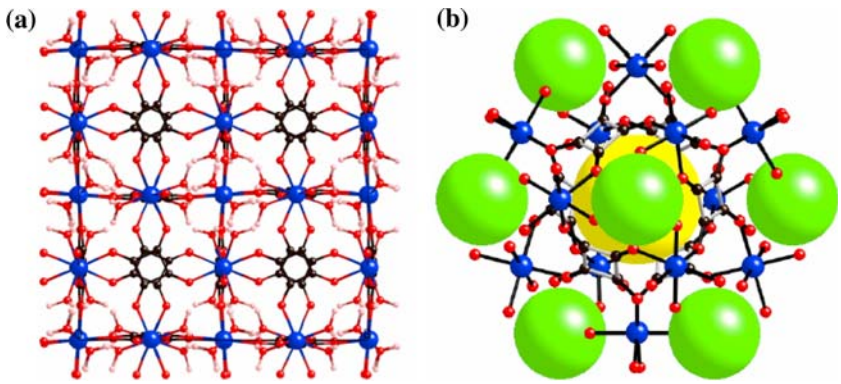

Fig. 1 Structure of **1**; (**a**) view of the unit cell along the c-axis and (**b**) along 111 showing the cavities in yellow and green spheres

oxygen atoms from four independent squarate and two water molecules. The octahedra are distorted (Table 2) with bond distances and angles in the range 2.042(5)–2.135(6) Å and 83.9(2)°–96.9(2)°, respectively. The network is generated by the *P* n-3n symmetry as shown in Fig. 1a. The most interesting part of the structure is the presence of two types of voids, a small one with a surface of water molecules and the large one with a surface of the planar cyclic C_4O_4 (Fig. 1b). Interestingly, both are completely empty as seen in the residual electronic densities. The estimated radii of the voids are 5 Å and 7 Å, respectively. Each squarate unit acts as a μ_4-bridge with Co–O–C–C–O–Co connections where the nearest Co–Co distance is 5.7 Å. The water molecules are connected by hydrogen bonding interaction to oxygen atoms of squarate ligands within the framework. Water molecules act as hydrogen donors and oxygen atoms of squarate ligands act as hydrogen acceptors.

The structural features of the framework are very similar to those reported for $M(C_4O_4)(H_2O)_2$, prepared by slow diffusion, in which acetic acid hydrate, water molecules or pyrazine molecules were suggested to incorporate into the void space as found by elemental analyses and single crystal structure determinations [30, 35]. However, the small residual electron densities (0.555 and −0.404 *e*/Å^3) in the Fourier difference map of **1** indicates that the spaces in the hydrothermally prepared crystals are empty. It is worth noting that the void space is not accessible because the squarate ligands function as windows to the boxes.

Crystal structure of **2**

We have recently reported the structure and magnetic properties of **2**, [29] thus we will only briefly describe them

Table 2 Selected bond distances (Å) and angles (°) for **1**

Co	O(1)	2.042(5)	Co	O(1′)	2.042(5)		
Co	O(2)	2.135(6)	Co	O(2′)	2.135(6)		
Co	O(3)	2.078(6)	Co	O(3′)	2.078(6)		
O(1)	Co	O(1′)	178.9(3)	O(1)	Co	O(2)	85.6(2)
O(1)	Co	O(2′)	93.7(2)	O(1)	Co	O(3)	83.9(2)
O(1)	Co	O(3′)	96.9(2)	O(1′)	Co	O(2)	93.7(2)
O(1′)	Co	O(2′)	85.6(2)	O(1′)	Co	O(3)	96.9(2)
O(1′)	Co	O(3′)	83.9(2)	O(2)	Co	O(2′)	93.0(3)
O(2)	Co	O(3)	88.2(2)	O(2)	Co	O(3′)	177.2(3)
O(2′)	Co	O(3′)	88.2(2)	O(3)	Co	O(3′)	90.8(3)

in relation to compounds **1** and **3**. Unlike the structure of **1** where each cobalt has two terminal water molecules in *trans*-positions, **2** has μ_3-hydroxide. In particular, there are two independent Co atoms (Fig. 2a), Co1 having two *trans*-OH and two Co2 having *cis*-OH, which are edge-shared distorted octahedra connected to one another to form ribbons of brucite, $Mg(OH)_2$. These ribbons are then bridged by μ_6-squarate to give the stable framework (Fig. 2b) with parallel channels filled with water molecules. These water molecules can be removed and re-inserted repeatedly without destroying the crystallinity of the crystals. Further details of this aspect can be obtained from reference [29]. Weak hydrogen bonds exist between the water molecules and between the water molecules and the surface atoms of the channels.

Crystal structure of **3**

Figure 3 shows the structure of **3** and the selected bond distances and angles are given in Table 3. The key feature of this compound is the presence of zigzag double chains, similar to those found in Goethite, FeOOH, and connected to one another into a stable framework by the squarate units. The structure is isostructural to that of the Mn analogue [36]. The chain consists of edge-sharing octahedra of Fe(II) where each distorted octahedron consists of three OH and three oxygen atoms from three independent squarate. Each OH acts as a μ_3-bridge to three Fe atoms and each μ_6-squarate connects six neighboring Fe atoms. Bond distances and angles (Table 3) are within the range 2.073(2)–2.106(2) Å and 81.56(9)°–106.39(9)°, respectively. Coordination mode of oxygen atoms of squarate is different from those found in **1** but similar to those of **2**. While O(2) coordinates to one Fe(II) ion, O(3) bridges two Fe(II) ions. The near-neighbor connections are Fe–O–Fe and Fe–O–C–C–O–Fe that are found in the structure of **2**. In contrast to the structures of **1** and **2**, the packing in **3** leaves no voids.

Crystal structure of **4**

The key feature in the structure of **4** (Fig. 4) is the parallel alignment of zigzag chains of Co-pydc along the *c*-axis and interpenetration of the benzene rings along the *b*-axis that results in cavities containing two water molecules per unit cell. There are two independent cobalt atoms and both have slightly distorted octahedral coordination (Table 4); Co1 has two water molecules, two carboxylate oxygen atoms and two pyridine nitrogen atoms while Co2 has four water molecules and two oxygen atoms from carboxylate. Interestingly, only one of the two carboxylate groups of each unit is coordinated to the metals. The pyridine nitrogen atom and one of the carboxylate oxygen atom chelates to form a five-atoms ring with the metal while the other oxygen atom binds to the second metal giving Co1–O–C–O–Co2 bridges. The interpenetration of the benzene rings is stabilized by π-π interaction of the type bond-over-ring with mean distance <3.4 Å.

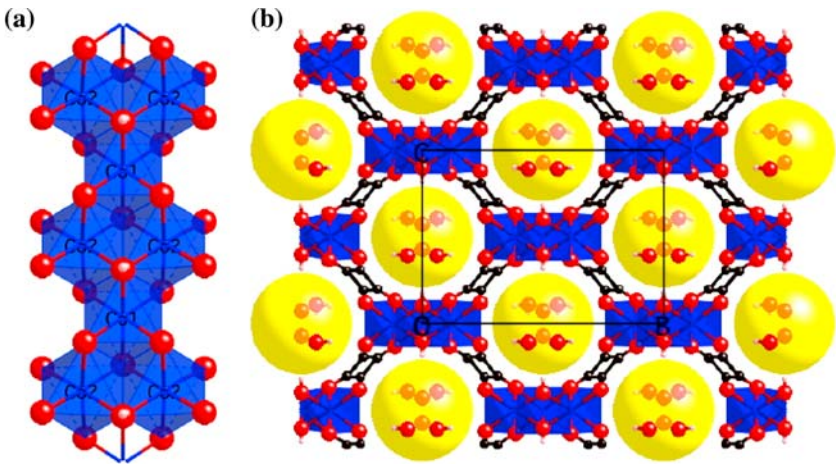

Fig. 2 Structure of **2**; (**a**) a single brucite ribbons of Co–OH and (**b**) view of the framework along the a-axis, showing the H_2O in the channels highlighted in yellow

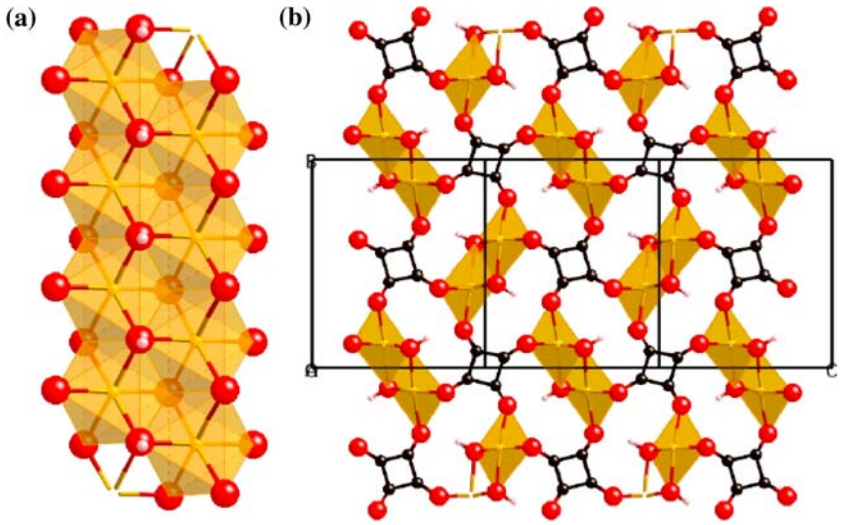

Fig. 3 Structure of **3**; (**a**) a single chain of Fe–OH similar to Goethite and (**b**) view of the framework along the a-axis

Table 3 Selected bond distances (Å) and angles (°) for **3**

Fe	O(1)	2.106(2)	Fe	O(1′)	2.101(2)		
Fe	O(1*)	2.073(2)	Fe	O(2)	2.077(2)		
O(1)	Fe	O(1′)	83.40(9)	O(1)	Fe	O(1*)	81.56(9)
O(1)	Fe	O(2)	174.78(8)	O(1′)	Fe	O(1*)	106.39(9)
O(1′)	Fe	O(2)	99.45(8)	O(1*)	Fe	O(2)	101.69(8)
Fe	O(1′)	Fe	96.60(9)	Fe	O(1*)	Fe	98.44(9)
Fe	O(1′)	Fe*	106.39(9)				

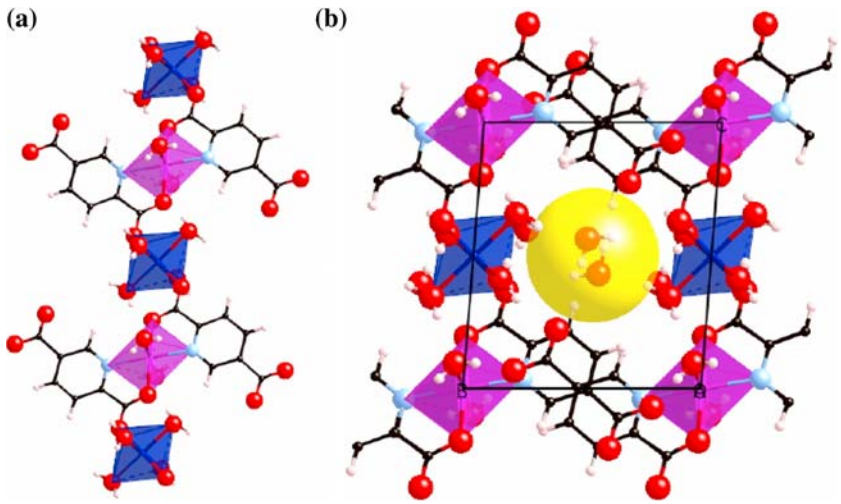

Fig. 4 Structure of **4**; (**a**) a single chain of Co-2,5-pydc and (**b**) view of the framework along the a-axis showing one cavity filled with two water molecules. The yellow circle represents the periphery of the cavity

Crystal structure of **5**

Like **4**, the key feature of the structure of **5** (Fig. 5) is the one-dimensional chain of Cu-pydc along the a-axis but unlike **4** it consists of only one independent copper, lying on a center of inversion, in a very Jahn-Teller distorted octahedral geometry—four oxygen atoms from four pydc and two pyridine nitrogen atoms (Table 5). Interestingly, only the donor atoms, two oxygen and one nitrogen atoms, on one side of the pydc make coordination bonds to the copper while the other two oxygen atoms are free; thus a bidendate O–CC–N and a monodentate O. There are no hydrogen bonds between the free oxygen and the hydrogen atoms. The packing of the chains is quite compact with no void space for solvents. The bridges between the copper atoms consist of five atoms, N–C–C–C–O and thus is not

Table 4 Selected bond distances (Å) and angles (°) for **4**

Co(1)	O(1)	2.063(2)	Co(1)	O(1′)	2.063(2)		
Co(1)	O(5)	2.104(2)	Co(1)	O(5′)	2.104(2)		
Co(1)	N(1)	2.126(2)	Co(1)	N(1′)	2.126(2)		
Co(2)	O(2)	2.085(2)	Co(2)	O(2′)	2.085(2)		
Co(2)	O(6)	2.078(2)	Co(2)	O(6′)	2.078(2)		
Co(2)	O(7)	2.101(2)	Co(2)	O(7′)	2.101(2)		
O(1)	Co(1)	O(1′)	180.0	O(1)	Co(1)	O(5)	88.91(7)
O(1)	Co(1)	O(5′)	91.09(7)	O(1)	Co(1)	N(1)	78.93(6)
O(1)	Co(1)	N(1′)	101.07(6)	O(1′)	Co(1)	O(5)	91.09(7)
O(1′)	Co(1)	O(5)	88.91(7)	O(1′)	Co(1)	N(1)	101.07(6)
O(1′)	Co(1)	N(1)	78.93(6)	O(5)	Co(1)	O(5′)	180.0
O(5)	Co(1)	N(1)	91.99(7)	O(5)	Co(1)	N(1′)	88.01(7)
O(5′)	Co(1)	N(1)	88.01(7)	O(5′)	Co(1)	N(1)	91.99(7)
N(1)	Co(1)	N(1′)	180.0	O(2)	Co(2)	O(2′)	180.0
O(2)	Co(2)	O(6)	88.98(7)	O(2)	Co(2)	O(6′)	91.02(7)
O(2)	Co(2)	O(7)	86.33(6)	O(2)	Co(2)	O(7′)	93.67(6)
O(2′)	Co(2)	O(6)	91.02(7)	O(2′)	Co(2)	O(6′)	88.98(7)
O(2′)	Co(2)	O(7)	93.67(6)	O(2′)	Co(2)	O(7′)	86.33(6)
O(6)	Co(2)	O(6′)	180.0(3)	O(6)	Co(2)	O(7)	89.13(8)
O(6)	Co(2)	O(7′)	90.87(8)	O(6′)	Co(2)	O(7)	90.87(8)
O(6′)	Co(2)	O(7′)	89.13(8)	O(7)	Co(2)	O(7′)	180.0

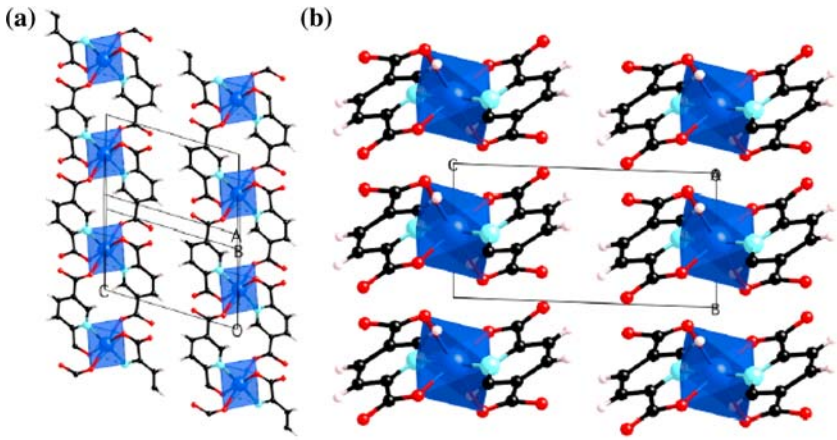

Fig. 5 Structure of **5** showing the parallel chains of Cu-2,5-pydc along the chain axis (a-axis) and perpendicular

expected to contribute to measurable magnetic exchange for the small $S = 1/2$ copper.

Magnetic properties

Temperature dependence of magnetic susceptibilities of **1–3** were measured in the temperature range 2–300 K in a fixed magnetic field and the isothermal magnetizations were measured in field of ±5 T at 2 K. The results are shown in Figs. 6–8, respectively.

For **1**, the effective moment decreases continuously and gradually on lowering the temperature; the slope being greater at low temperatures. Fitting of the inverse susceptibility to the Curie-Weiss function for data above 100 K gives a Curie constant of 3.013(4) emu K mol^{-1} and a Weiss constant of −7.2(4) K. The effective magnetic moment of **1** (4.91 μ_B) is consistent with that expected for octahedral Co(II) ion. The value are typical for Co(II) ion in an octahedral environment with an enhanced moment due to orbital contribution and a lowering of the moment at low temperature due to effect of spin-orbit coupling. The isothermal magnetization at 2 K exhibits a continuous increase to a saturation value of 2.4 μ_B per Co(II). The saturation value is within the range expected for Co(II) with effective $S = 1/2$ and anisotropic g-values (average of

Table 5 Selected bond distances (Å) and angles (°) for **5**

Cu(1)	O(1)	1.931(2)	
Cu(1)	O(4)	2.696(2)	
Cu(1)	N(1)	1.972(3)	
O(1)	Cu(1)	N(1)	83.2(1)
O(1)	Cu(1)	O(4)	81.5(1)
O(4)	Cu(1)	N(1)	80.9(1)

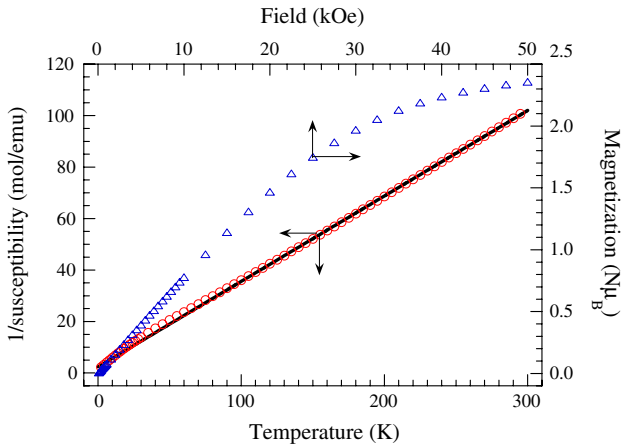

Fig. 6 Temperature dependence of the inverse susceptibility (circles), the Curie-Weiss fit (black line) and the isothermal magnetization (triangles) at 2 K for **1**

4.3). The value of the Weiss constant suggests weakly interacting Co(II) ions.

For **2**, the results have been reported before [29] and it only suffice to add here for reference that the virgin sample behaves as ferromagnetic chains (C = 9.91(2) emu K mol^{-1} and a Weiss constant of 0.2(3) K), which are antiferromagnetically coupled to one another to give a 3D long-ranged Néel state below 8 K (Fig. 7). However, the weak coupling between the ferromagnetic chains can be overcome to give a ferromagnetic state above the metamagnetic critical field of 1200 Oe. However, due to the high anisotropy of Co(II) a small canting is observed. Upon dehydration, the ferromagnetic chains are now ferromagnetically coupled to one another to give a 3D long-range ferromagnetic ordering at 8 K. The presence of the ferromagnetic state is confirmed by the observation of a sharp peak in both the real and imaginary parts of the ac-susceptibilities (Fig. 7 insert). Upon rehydration of the sample, the magnetization data suggest that the virgin state is restored. This process is reproducibly reversible.

Compound **1** and **2** exhibit not only different color of crystals but also different magnetic properties. The difference in color being due to the different octahedral distortions while for the magnetic properties it is due to the connectivity between Co(II) ions in the structures. While both have Co–O–C–C–O–Co bridges that contribute to

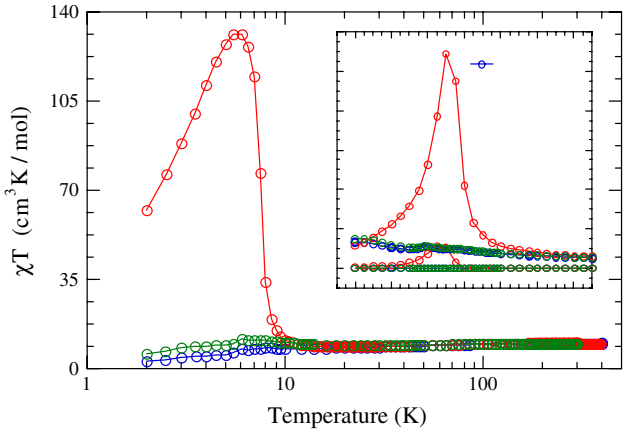

Fig. 7 Temperature dependence of the products of susceptibility and temperature (circles) of the virgin (blue), dehydrated (red) and rehydrated (green) of **2**. Insert shows the corresponding ac-susceptibilities

weak exchange interactions between nearest-neighbors, **2** has in addition Co–O–Co bridges that introduce stronger exchange interactions. Consequently, for the latter short-range correlation results in large effective moment within the chains that need only a weak coupling between these large moments to achieve long-range ordering. Furthermore, the structure of **2** consists of brucite-like ribbons of formula $[Co^{II}_3(\mu\text{-}OH)_2]^{4+}$ that is commonly found to be ferromagnetic due to the edge-sharing of the octahedral [29, 22]. Therefore, the lack of magnetic interaction in **1** is due to absence of single-atom bridge and short Co(II)–Co(II) distance.

A proper study of the magnetic properties of **3** was not possible due to the presence of magnetic iron-oxide particles. However, the temperature dependence of the susceptibility shows a long range magnetic ordering at 15 K (Fig. 8) and a possible field-induced transformation (spin-flop or metamagnetic critical field) at ca 45 kOe at

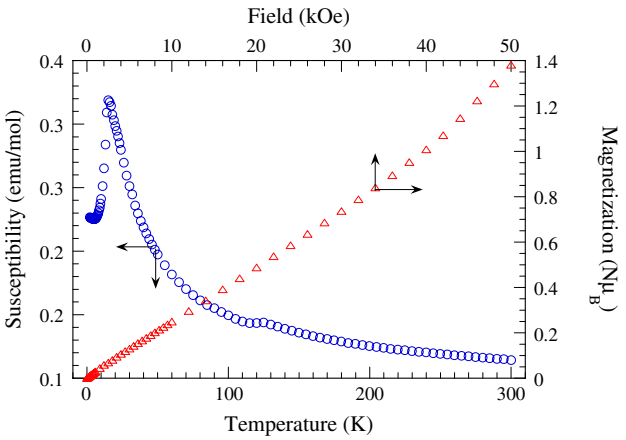

Fig. 8 Temperature dependence of the susceptibility (circles) and the isothermal magnetization (triangles) at 2 K for **3**

2 K. In relation to the above observation for **2**, the long-range ordering for **3** is likely of the same nature as **2**. However, the lack of an estimation of the Weiss constant does not permit us to derive a mechanism of the long-range magnetic ordering of this compound.

Conclusion

Several different structural coordination polymeric phases are obtained from the hydrothermal reactions of M(II) (M = Fe or Co) and squaric acid which suggests there are more underlying factors to be mastered in controlling the final products. Single crystal structures confirm that M–O–M connections, as well as the presence of μ_3-OH, are important for long-range magnetic ordering. However, the final arrangements and electronic and spin states of M(II) have important consequence on the type of magnetic ordering. The importance of magnetic exchange through hydrogen-bond is revealed for the first time by the transformation of a ferrimagnet for a hydrate to a ferromagnet for the non-hydrate. Insertion of other solvents in under way to understand these subtle differences resulting in different ground-states. However, the combined coordination of pyridine and carboxylate of pyridinedicarboxylate does not result in structures of interest in magnetism.

Acknowledgement This work was funded by the CNRS-France, Ministry of Education, Science, Sports, and Culture, Japan. H.K. thanks the JSPS for a Young Scientist Fellowship.

References

1. Kitagawa S, Kitaura R, Noro S (2004) Angew Chem Int Ed 43:2334
2. Kepert CJ (2006) Chem Commun 695
3. Day P, Kurmoo M (1997) J Mater Chem 7:1291
4. Kobayashi H, Sato A, Arai E, Akutsu H, Kobayashi A, Cassoux P (1997) J Am Chem Soc 119:12392
5. Halder GJ, Kepert CJ, Moubaraki B, Murray KS, Cashion JD (2002) Science 298:1762
6. Kurmoo M, Graham AW, Day P, Coles SJ, Hursthouse MB, Caulfield JL, Singleton J, Francis JP, Hayes W, Ducasse L, Guionneau P (1995) J Am Chem Soc 117:12209
7. Mori W, Takamizawa S (2000) J Solid State Chem 152:120
8. Kitagawa S, Kondo M (1998) Bull Chem Soc Jpn 71:1739
9. Biradha K, Fujita M (2002) Angew Chem Int Ed 41:3392
10. Wang Z-M, Zhang B, Fujiwara H, Kobayashi H, Kurmoo M (2004) Chem Commun 416
11. Yamada K, Yagishita S, Tanaka H, Tohyama K, Adachi K, Kaizaki S, Kumagai H, Inoue K, Kitaura R, Chang H-C, Kitagawa S, Kawata S (2004) Chem Eur J 10:1
12. Kurmoo M, Kumagai H, Green MA, Lovett BW, Blundell SJ, Ardavan A (2001) J Solid State Chem 159:343
13. Kumagai H, Oka Y, Tanaka M-A, Inoue K (2002) Inorg Chim Acta 332:176
14. Kumagai H, Chapmann KM, Kepert CJ, Kurmoo M (2003) Polyhedron 22:1921
15. Kumagai H, Kepert CJ, Kurmoo M (2002) Inorg Chem 41:3410
16. Rujiwatra A, Kepert CJ, Claridge JB, Rosseinsky MJ, Kumagai H, Kurmoo M (2001) J Am Chem Soc 123:10584
17. Kumagai H, Oka Y, Inoue K, Kurmoo M (2002) J Chem Soc Dalton Trans 3442
18. Kumagai H, Ohba M, Inoue K, Okawa H (2002) Chem Lett 1006
19. Kumagai H, Akita-Tanaka M, Kawata S, Inoue K (2005) Chem Lett 526
20. Kurmoo M, Kumagai H (2002) Mol Cryst Liq Cryst 397:555
21. Kumagai H, Oka Y, Inoue K, Kurmoo M (2004) J Phys Chem Solid 65:55
22. Kurmoo M, Kumagai H, Hughes SM, Kepert CJ (2003) Inorg Chem 42:6709
23. Kumagai H, Akita-Tanaka M, Inoue K, Kurmoo M (2001) J Mater Chem 11:2146
24. (a) Kumagai H, Inoue K, Kurmoo M (2002) Bull Chem Soc Jpn 75:1282 (b) Kurmoo M, Estournes C, Oka Y, Kumagai H, Inoue K (2005) Inorg Chem 44:217
25. Kurmoo M (1999) Chem Mater 11:3370
26. Kurmoo M (1999) Phil Trans A 357:3041
27. Kurmoo M (1999) J Mater Chem 9:2595
28. Kurmoo M, Kumagai H, Akita-Tanaka M, Inoue K, Takagi S (2006) Inorg Chem 45:1627
29. Kurmoo M, Kumagai H, Chapman KW, Kepert CJ (2006) Chem Commun 3012
30. Robl C, Weiss A (1986) Z Naturforsch 41B:1341
31. Kawata S, Kitagawa S, Kumagai H, Ishiyma T, Honda K, Tobita H, Adachi K, Katada M (1998) Chem Mater 10:3902
32. Gutschke SOH, Molinier M, Powell AK, Wood PW (1997) Angew Chem Int Ed 36:991
33. Lee C-R, Wang C-C, Chen K-C, Lee G, Wang YJ (1999) Phys Chem A103:156
34. Yaghi OM, Li G, Groy TL (1995) J Chem Soc Dalton Trans
35. Weiss A, Riegler E, Alt I, Bohme H, Robl CZ (1986) Naturforsch 41B:18
36. Yufit DS, Price DJ, Howard JAK, Gutschke SOH, Powell AK, Wood PT (1999) Chem Commun 1561
37. Hagrman PJ, Hagrman D, Zubieta J (1999) Angew Chem Int Ed 38:2638
38. Gutschke SOH, Molinier M, Powell AK, Wood PW (1997) Angew Chem Int Ed Engl 36:991
39. Lin KJ, Lii KH (1997) Angew Chem Int Ed Engl 36:2076
40. Sheldrick GM (1985) Crystallographic computing 3. Oxford University Press